RESEARCH PAPER

Theoretical and Experimental Investigation of Optical Properties of ZnS Zig-Zag Thin Films

M. Minbashi, R. Zarei Moghadam*, M. H. Ehsani, H. R. Dizaji and M. K. Omrani

** r.zarei1991@semnan.ac.ir*

Received: April 2018 **Revised: August 2018** **Accepted: October 2018**

Thin Film Lab, Faculty of Physics, Semnan University, Semnan, Iran.

DOI: 10.22068/ijmse.16.2.67

Abstract: *Zigzag ZnS thin films prepared by the thermal evaporation method using glancing angle deposition (GLAD) technique. ZnS films with the zigzag structure were produced at deposition angles of 0˚, 70˚ and 80˚ at room temperature on glass substrates. Surface morphology of the films was characterized by using field emission scanning electron microscopy (FESEM). The optical properties of the specimens were investigated by using UV-Vis spectroscopy technique. To characterize the porosity of the simulated structures, the PoreSTAT software which analyses the NASCAM software was employed. The optical transmissions of the samples were calculated by using NASCAM optics package. The simulation results are completely in agreement with the experimental results.*

Keywords: *Zigzag, ZnS thin film, Glancing angle deposition, Optical properties.*

1. INTRODUCTION

Glancing angle deposition (GLAD) method is based on physical vapor deposition and employs oblique angle deposition conditions as well as substrate rotation, fabricating and engineering microstructures by an atomic shadowing effect [1-3]. The first experiment using GLAD method was carried out in 1959. Young and Kowal [4] in 1959 first fabricated inorganic thin film onto a rotating substrate around the normal axis. In 1966, Nieuwenhuizen and Haanstra [5] deliberately changed the substrate tilt with respect to the average direction of the incident vapor flux once during deposition. The substrate position in a GLAD process is specified by two angles (Fig. 1). The deposition angle α is defined as the angle between the substrate normal and the incident vapor flux direction. Fig. 1 shows the schematic diagram set-up for GLAD motion control wherein, the substrate is mounted on a rotating stage with two angles. The α motor controls the substrate tilt and the φ motor rotates the substrate about its normal. The α angle can vary between 0◦ (normal incidence) and 90◦ (parallel to the substrate), whereas the φ angle can assume any value and is periodic [6]. The following six structures are all deposited using different GLAD processes designed to manipulate the ballistic shadowing conditions during growth process in different ways: zigzag structures, helical structures, vertical columns, graded-density structures, periodic structure arrays, and hollow-core structures. The GLAD technique has also been used to fabricate high-surface-area support structures using various materials such as C [7], Cr [8], CrN [9], Nb2O5 [10] and Ti [11].

The microstructure of the GLAD thin films can be controlled by varying the orientation of rotating substrate during deposition. There are various applications for the films produced by GLAD technique, such as anisotropic antireflection coating [12], three-dimensional photonic crystals [13], optical filters [14], birefringent omnidirectional reflectors [15], linear polarizer [16], and fluid concentration sensing [16], etc.

Zinc sulfide (ZnS) is an important and belongs to II–VI compound semiconductors material with a wide bandgap (3.6–3.9 eV) [17, 18]. It has a refractive index of 2.2 at a wavelength of 10 μm and a reflection loss of 24.7% [19]. ZnS thin films are used as flat-panel display [20] antireflection coating [19], dielectric filter [21], electroluminescence thin films [22] photodetectors [23], short-wavelength emitting laser diodes [24], etc. ZnS films have prepared with various deposition techniques such as thermal evaporation [25], pulsed laser deposition (PLD) [26],

[DOI: 10.22068/ijmse.16.3.67]

electron beam evaporation [27], chemical vapor deposition (CVD) [28], etc. After going through the available results obtained for ZnS thin films employing various treatments, a curiosity to use these thin films as a buffer layer to thin-film solar cells is achieved. Since ZnS thin films as buffer layer with the application of annealing in air atmosphere are not well-understood, therefore, in this communication, the physical properties of ZnS thin films have been optimized by post-annealing treatment within the temperature range of 100-500 °C for solar cell applications as buffer layer [29].

Various models have been developed to simulate and predict the evolution of thin-film morphology. Some of these models are: geometric models [30], continuum models [31-33], ballistic aggregation models [34-36] and molecular dynamics models [37]. Therefore, a ballistic aggregation Monte Carlo simulation has been used to understand the influence of atomistic processes on the formation of the film nanostructure during growth. More complex and realistic diffusion kinetics can be simulated by different methods. Smy et al. [38] allow deposited particles to diffuse short distances according to curvature-dependent chemical potential. Karabacak et al. modeled the diffusion process by allowing a fixed number of random particle hops after aggregation [39].

In this work, NASCAM software [40] has been used to analyze film growth. This widely employed computer code has already helped to explain numerous issues regarding the kinetic energy of the vapor particles, the bond structure and chemical nature of the films.

In this paper, the effect of the deposition angle on the anisotropic optical properties of ZnS zigzag thin films fabricated by GLAD technique is reported. transmission spectra of ZnS films with the zigzag structure were studied by using a theoretical model and the results were compared with the experimental ones. The s and p-refractive indices, the porosity, and the in-plane birefringence at various deposition angles are described.

In addition, the optical properties of GLAD ZnS zigzag nanostructured thin films grown using various incident angles α=0, 70°, and 80° each with a nominal thickness of 300 nm were investigated.

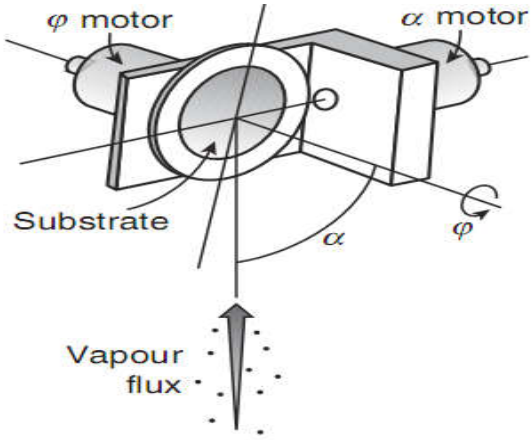

Fig. 1. Schematic diagram showing set-up for GLAD motion control wherein the substrate is mounted on a rotating stage with two angles. The α motor controls the substrate tilt and φ motor rotates the substrate about its normal [6].

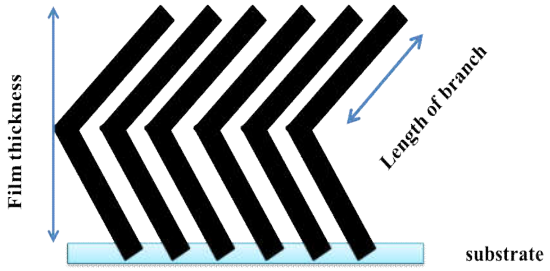

Fig. 2. The schematic showing substrate, length of branches and film thickness of ZnS zigzag films.

2. EXPERIMENTAL

ZnS nanostructured films were deposited by the thermal evaporation method on glass substrates in Hind-HIVAC coating (Model ISF6) equipped with GLAD technique. Two stepper motors were introduced into the deposition system to tilt and rotate the substrate automatically, as shown in Fig. 1. The α motor controls the substrate tilt, while the φ motor rotates the substrate about its normal [6]. High purity ZnS (99.99%) in the form of tablets, supplied by Sigma - Aldrich Company, was used as an evaporation source material in a molybdenum boat. Before deposition, the glass substrates were cleaned by use of deionized water, acetone, and ethanol for 20 min in an ultrasonic bath and dried with purified nitrogen gas. The deposition rate and the thickness of the films

[DOI: 10.22068/ijmse.16.3.67]

were calculated and controlled in-situ for a non-angled and non-rotating substrate by a quartz-crystal sensor (Model DTM-101) placed near the substrate. The average evaporation rate was maintained at 2 Å/s. The chamber pressure was maintained about 10^{-5} mbar. Deposition of the thin films was performed at room temperature. The distance between the evaporation source and the glass substrate was 30 cm.

To produce zigzag films, the first branch was deposited on the substrate at a fixed incident angle. For producing the second branch, the film was rotated by 180° without opening the vacuum chamber. This was done using a mechanical attachment enabling the operator to rotate the substrate by 180° from outside the vacuum unit. The schematic showing substrate, length of branches, and film thickness of ZnS zigzag films shown in Fig. 2. In this paper, ZnS zigzag films were prepared with the same nominal branch thicknesses at various incident flow angles of 0, 70˚, and 80˚ which are labeled as S0, S70, and S80. The nominal growth characteristic of the S0, S70, and S80 samples are given in Table 1.

Table. 1. Nominal growth characteristics of the S0, S70 and S80 samples.

Sample	Deposition angle (degree)	Length of each branch (nm)
S0	0	600
S70	70	2×300
S80	80	2×300

The prepared samples were studied by the following device. Optical transmittance was calculated by using UV-Vis Lambda900 spectrophotometer in the wavelength range of 350 to 850 nm. The cross-section and surface morphology of the films were characterized by using field emission scanning electron microscopy (FESEM).

3. GROWTH MODEL AND PORE ANALYSIS OF SIMULATED FILMS

In the present study, the growth of the ZnS GLAD films was simulated by using NASCAM Software. This code is developed to simulate the time evolution of atoms deposited on a substrate. It is based on the kinetic Monte Carlo (kMC) method. kMC can be used for modeling different processes occurring at the surface, such as the growth of films during deposition or the development of films post deposit at the atomic scale. Once the particles arrive at the film surface, different mechanisms and surface mobility processes are induced depending on the energy of the particles and the local bond structure [40]. The goal of the kMC method is to mimic real experiments through simulations. Because kMC does not take into account the vibrational movement of atoms it is possible to use kMC to model the evolution of a system for longer periods of time, unlike the Molecular Dynamics simulation which can only be used to simulate the dynamics of a system for a short period of time, about 10^{-9} s. Depending on the number of atoms in the system, along with some other parameters such as temperature and atomic properties, the physical time might be hundreds to thousands of seconds. The energy and angular distribution of incident particles were calculated by SRIM [40] and SIMTRA codes. First, SRIM is used to calculate the energy and the direction of the particles leaving the target. The particles are then transported in the gas phase by the SIMTRA code which takes into account all the collisions between the sputtered species and the gas molecules.

The porous structure of simulated thin films was analyzed by considering cross-section view of the material. For the pore analysis of the thin films, the PORESTAT software developed for NASCAM simulation analysis was used. NASCAM optics package is used to simulate the optical properties of different materials. Using this package, one can determine some features of materials after simulation like roughness, the density of coating, mean diffusion path, substrate coverage, porosity shown with PoreSTAT software, and etc.

After performing the simulation, the output of NASCAM package has to be used by another program (the PoreSTAT software) to understand the optical properties of this ma-

[DOI: 10.22068/ijmse.16.3.67]

terial. Since porosity has an important role in optical properties of GLAD thin films, therefore the obtained porosity data were then used as the input data of NASCAM optics package. The theory used for these simulations was based on Bruggeman's effective medium theory. Since pore sizes (mesopores) are much lower than visible-range wavelengths, Bruggeman's effective medium theory [41, 42] can be used to calculate the effective permittivity (ε_{eff}). This modeling was employed in this paper to evaluate the fraction of ZnS as a function of film depth to determine the dependence of the refractive index on the film depth (index profile). According to Bruggeman's theory:

$$q(z)\frac{n_{ZnS}^2-n_{eff}^2}{n_{ZnS}^2+2n_{eff}^2}+[1-q(z)]\frac{1-n_{eff}^2}{1+2n_{eff}^2}=0 \qquad (1)$$

Where n_{ZnS}^2 is the refractive index of the dense ZnS film and n_{eff} is the effective refractive index of a blend of a dense ZnS material and voids filled with air. q(z) represents the volume filling fraction of the ZnS film which varies with the film depth z into the porous thin film [43]. The function q(z) and the film thickness were determined using the numerical procedure developed for the optimization of the continuous refractive index profiles [44].

4. RESULTS AND DISCUSSION

4.1. Theoretical and experimental of the Cross-section

Simulation and cross-sectional FESEM images of the ZnS zigzag thin films for S0, S70, and S80 samples are shown in Fig. 3. The zigzag structure formation of the ZnS thin films is made by rotating the substrate by 180˚ around its normal axis. A clear column tapering observed in FESEM images are due to the shadowing effect as reported by others [45, 46].

The following equations give the relation between the incident flux angle (α) and columnar angle (β) [47]:

$$tan\beta=\frac{1}{2}tan\alpha \qquad \text{For } \alpha<0 \qquad (2)$$

$$\beta=\alpha-sin^{-1}\left(\frac{1-cos\alpha}{2}\right) \qquad \text{For } \alpha>0 \qquad (3)$$

Using the ImageJ software, the β values and columns thickness was calculated from the cross-sectional FESEM images. The β values were found equal to 45˚ and 55˚ for samples S70 and S80, respectively. A good agreement is found between the calculated results using the Eqs. 2, 3, and the obtained values by using the software. The calculated angle, actual angle and actual thickness for S0, S70, and S80 samples have been measured by using cross-sectional FESEM images and presented in Table. 2. Considering the growth behavior of columns shown in Fig. 3, one can easily observe that the column diameter is bigger at its top than its bottom. This kind of column tapering may be due to the shadowing effect.

To characterize the porosity of the simulated structures, the PoreSTAT software which analyses the NASCAM files and performs a full 3D analysis of the porous structure of the thin films has been used [48, 49]. The total number of effective particles in the simulation was taken as 500000 with a simulated film thickness of about 580.35 nm. The results show that the porosity increases upon increasing the growth angle of growth. The calculated porosity of the structures of the zigzag ZnS thin films for S70 and S80 samples are 49.5%, 67.2%, respectively. The results obtained by using the PoreSTAT software for S0, S70, and S80 samples are shown in Fig. 3. The figures drawn using the simulation results for any specimen is found very resemble their corresponding FESEM image.

Table. 2. results obtained by using cross-sectional FESEM images for S0, S70, and S80 samples

samples	Calculated angle (degree)	Actual angle (degree)	Actual thickness (nm)
S0	0	0	600
S70	45	38	450
S80	55	50	200

[DOI: 10.22068/ijmse.16.3.67]

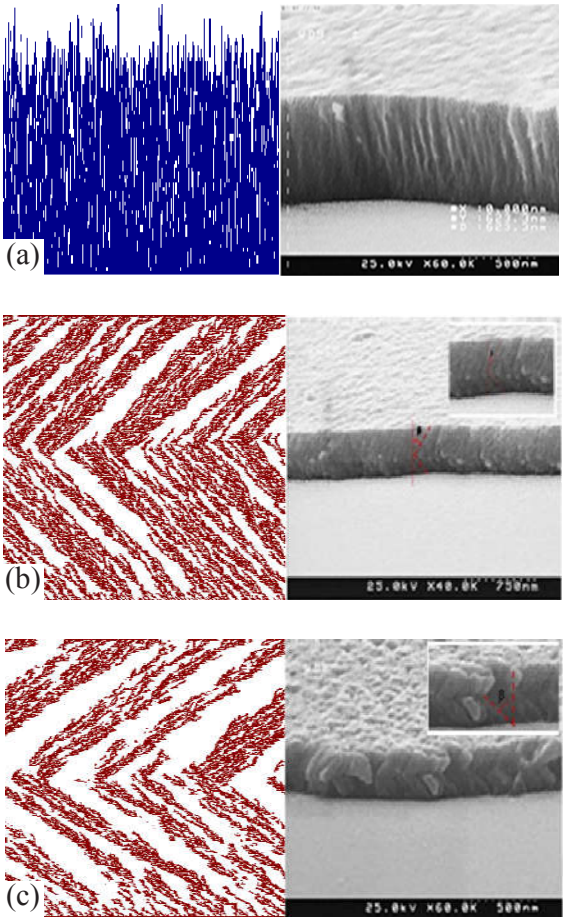

Fig. 3. Simulation (left) and cross-sectional FESEM images (right) of (a) S0, (b) S70 and (c) S80 samples.

4.2. Optical Properties of the GLAD Films

To investigate the optical properties of the zigzag ZnS thin films, the transmission spectra of samples were obtained by UV-Vis spectrophotometer in the wavelength range of 350 to 850 nm. The transmittance spectra for S0 (a), S70 (b), and S80 (c) samples are shown in Fig. 4. The transmission of samples was calculated by using NASCAM optics package based on Bruggeman's effective medium theory. The results show that by increasing the growth angle, optical transmission of the zigzag ZnS thin films increased. It was shown in the preview section that increasing the growth angle would lead to increase the film porosity, hence one may find a direct relationship between the film porosity and its transmission. The measured transmission spectra are in excellent agreement with the calculated spectra for S0 (a), S70 (b), and S80 (c) samples. By comparing the two spectra shown in Fig. 4, one finds very good agreement between the experimental and theoretical findings.

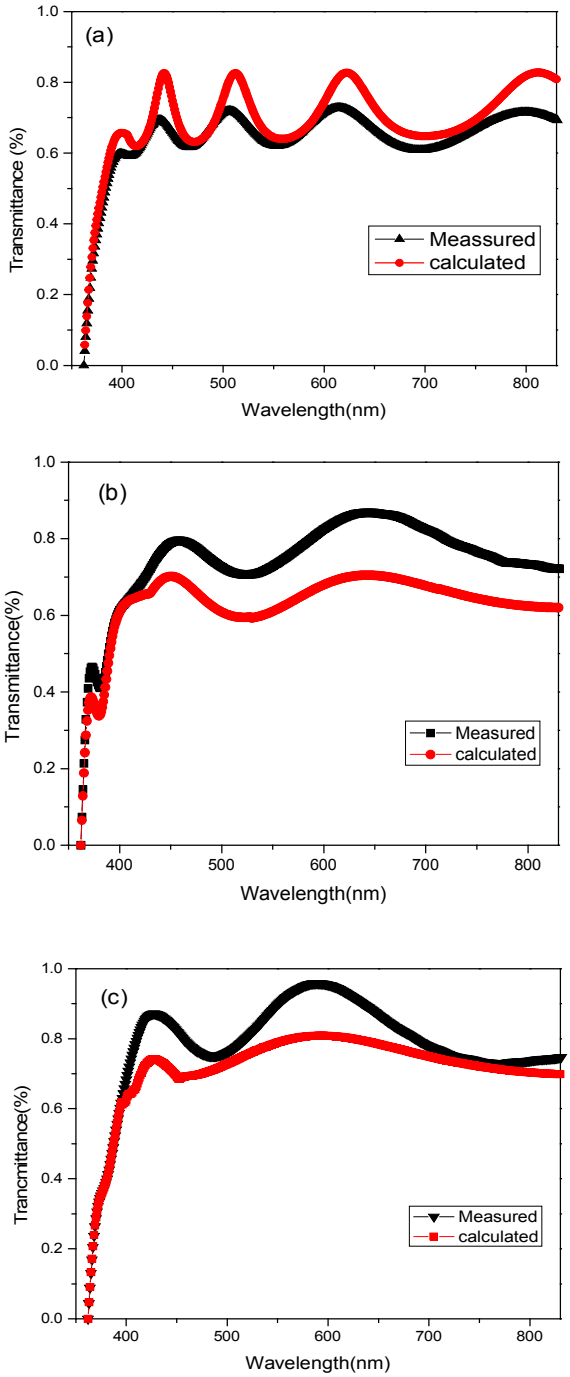

Fig. 4. Measured and calculated transmittance of S0 (a), S70 (b), and S80 (c) samples versus wavelength.

[DOI: 10.22068/ijmse.16.3.67]

5. CONCLUSION

Zigzag ZnS thin films were produced by thermal evaporation method on the glass substrate at room temperature by using glancing angle deposition (GLAD) technique. The samples were prepared at different growth angles 0˚, 70˚, and 80˚. The morphological studies of the ZnS films prepared at 70˚ and 80˚ deposition angles confirmed the formation of the zigzag shape. The transmission spectra of samples were measured experimentally and calculated theoretically by using NASCAM optics package and good agreement was observed between the results. The calculated porosity of the structures of the zigzag ZnS thin films for S70 and S80 samples are 49.5%, 67.2%, respectively.

REFERENCES

1. Park, Y. J., Sobahan, K. and Hwangbo, C. K. "Wideband circular polarization reflector fabricated by glancing angle deposition," Optics express, 2008, 16, 5186-5192.
2. Woo, S. H. and Hwangbo, C. K. "Optical anisotropy of microstructure-controlled TiO_2 films fabricated by glancing-angle deposition (GLAD)," Journal of the Korean Physical Society, 2006, 48, 1199-1204.
3. Robbie, K. Sit, J. and Brett, M. "Advanced techniques for glancing angle deposition," Vacuum Science & Technology B, 1998, 16, 1115-1122.
4. Young N. O. and Kowal, J. "Optically active fluorite films," Nature, 1959, 183, 104-105.
5. Nieuwenhuizen J. and HAANSTRA H., "Microfractography of thin films," Philips Tech Rev, 1966, 27, 87-91,.
6. Hawkeye, M. M., Taschuk, M. T., and Brett, M. J., Glancing angle deposition of thin films: engineering the nanoscale: John Wiley & Sons, 2014, 41 - 49.
7. Gasda, M., Eisman, G. and Gall, D., "Nanorod PEM fuel cell cathodes with controlled porosity," Journal of the Electrochemical Society, 2010, 157, 437-440.
8. Khudhayer, W. J., Kariuki, N., Myers, D. J., Shaikh, A. U., and Karabacak, T., "GLAD Cr nanorods coated with SAD Pt thin film for oxygen reduction reaction," Journal of the Electrochemical Society, 2012, 159, 729-736.
9. Gasda, M., Eisman, G. and Gall, D. "Sputter-deposited Pt/CrN nanoparticle PEM fuel cell cathodes: limited proton conductivity through electrode dewetting," Journal of The Electrochemical Society, 2010, 157, 71-76.
10. Bonakdarpour, A., Tucker, R. T., Fleischauer, M. D., Beckers, N. A., Brett, M. J. and Wilkinson, D. P. "Nanopillar niobium oxides as support structures for oxygen reduction electrocatalysts," Electrochimica Acta, 2012, 85, 492-500.
11. Bonakdarpour, A., Fleischauer, M., Brett, M. and Dahn, J. "Columnar support structures for oxygen reduction electrocatalysts prepared by glancing angle deposition," Applied Catalysis A: General, 2008, 349, 110-115.
12. Chhajed, S. Schubert, M. F., Schubert, E. F. and Kim, J. "Nanostructured multilayer graded-index antireflection coating for Si solar cells with broadband and omnidirectional characteristics," 2008, 93, 251108.
13. Lakhtakia A. and Messier R., Sculptured thin films: nanoengineered morphology and optics SPIE press Bellingham, WA, 2005, 122, 25-45.
14. Hodgkinson I. and Wilson P. W., "Microstructural-induced anisotropy in thin films for optical applications," Critical Reviews in Solid State and Material Sciences, 1988, 15, 27-61.
15. Kaminska K. and Robbie, K. "Birefringent omnidirectional reflector," Applied optics, 2004 43, 1570-1576.
16. Wu, Q. H., De Silva, L., Arnold, M., Hodgkinson, I. J. and Takeuchi, E. "All-silicon polarizing filters for near-infrared wavelengths," Journal of applied physics, 2004, 95, 402-404.
17. Tajik, N., Ehsani, M. H., Moghadam, R. Z., Dizaji, H. R. "Effect of GLAD technique on optical properties of ZnS multilayer antireflection coatings. Materials Research Bulletin. 2017, 100, 265-274.
18. Ashrafi, M. M. A., Dizaji, H. R., Ehsani, M. and Moghadam, R. Z., "Zns Film Properties Modification Using Oblique Angle Deposition Technique'. Surface Review and Letters, 2017, 1850119-9.
19. Moghadam, R. Z., Ahmadvand, H. and Jannesari, M. "Design and fabrication of multi-layers infrared antireflection coating consisting of

[DOI: 10.22068/ijmse.16.3.67]

ZnS and Ge on ZnS substrate," Infrared Physics & Technology, 2016, 75, 18-21.
20. Tong, W., Tran, T., Park, W., Schön, S., Wagner, B. and Summers, C. "High-quality ZnS thin-film growth for flat-panel displays," Journal of the Society for Information Display, 1996, 4, 325-329.
21. Ruffner, J. A., Himel, M. D., Mizrahi, V., Stegeman, G. I. and Gibson, U. J. "Effects of low substrate temperature and ion assisted deposition on composition, optical properties, and stress of ZnS thin films," Applied optics, 1989, 28, 5209-5214.
22. Keir, P., Maddix, C., Baukol, B., Wager, J., Clark, B. and Keszler, D. "Lanthanide doping in ZnS and SrS thin-film electroluminescent devices," Journal of Applied Physics, 1999, 86, 6810-6815,.
23. Dai, J., Song, X., Zheng, H., and Wu, C. "Excitonic photoluminescence and photoresponse of ZnS nanowires," Materials Chemistry and Physics, 2016, 174, 204-208.
24. Zhang, W., Zeng, X., Lu, J. and Chen, H. "Phase controlled synthesis and optical properties of ZnS thin films by pulsed laser deposition," Materials Research Bulletin, 2013, 48, 3843-3846.
25. Prathap, P., Subbaiah, Y. V., Reddy, K. R. and Miles, R. "Influence of growth rate on microstructure and optoelectronic behaviour of ZnS films," Journal of Physics D: Applied Physics, 2007, 40, 5275.
26. Hillie K. and Swart, H. "Effects of SnO 2 surface coating on the degradation of ZnS thin film phosphor," Applied surface science, 2007, 253, 8513-8516.
27. Wang, S., Fu, X., Xia, G., Wang, J., Shao, J. and Fan, Z., "Structure and optical properties of ZnS thin films grown by glancing angle deposition," Applied surface science, 2006, 252, 8734-8737.
28. Zhang, Z., Shen, D., Zhang, J., Shan, C., Lu, Y., Liu, Y., "The growth of single cubic phase ZnS thin films on silica glass by plasma-assisted metalorganic chemical vapor deposition," Thin Solid Films, 2006, 513, 114-117.
29. Patel, S.L., Purohit, A., Chander, S. and Dhaka, M.S.,. Thermal annealing evolution to physical properties of ZnS thin films as buffer layer for solar cell applications. Physica E: Low-dimensional Systems and Nanostructures, 2018, 101,174-177.
30. Yang, B., Walden, B. L., Messier, R. and White, W. B. "Computer simulation of the cross-sectional morphology of thin films," in 31st Annual Technical Symposium, 1988, 68-76.
31. S. Hamaguchi and S. Rossnagel, "Surface-topography simulations of ionized sputter metal deposition," in MRS Proceedings, 1995, p. 113.
32. Hamaguchi S. and Rossnagel, S. "Simulations of trench-filling profiles under ionized magnetron sputter metal deposition," Journal of Vacuum Science & Technology B, 1995, 13, 183-191.
33. Hamaguchi S. and Rossnagel, S. "Liner conformality in ionized magnetron sputter metal deposition processes," Journal of Vacuum Science & Technology B, 1996, 14, 2603-2608.
34. Messier, R., Venugopal, V. C., and Sunal, P. D. "Origin and evolution of sculptured thin films," Journal of Vacuum Science & Technology A, 2000, 18, 1538-1545.
35. Dirks A. and Leamy, H. "Columnar microstructure in vapor-deposited thin films," Thin Solid Films, 1977, 47, 219-233.
36. Meakin, P., "Ballistic deposition onto inclined surfaces," Physical Review A, 1988, 38, 994.
37. Sherwin J. and Lakhtakia, A. "Nominal model for structure-property relations of chiral dielectric sculptured thin films," Mathematical and computer modelling, 2001, 34, 1499-1514.
38. Smy, T., Vick, D., Brett, M., Dew, S., Wu, A., Sit, J., "Three-dimensional simulation of film microstructure produced by glancing angle deposition," Journal of Vacuum Science & Technology A, 2000, 18, 2507-2512.
39. Karabacak, T., Singh, J., Zhao, Y.-P., Wang, G.-C. and Lu, T.-M., "Scaling during shadowing growth of isolated nanocolumns," Physical Review B, 2003, 68, 125408-5.
40. Lucas S. and Moskovkin, P. "Simulation at high temperature of atomic deposition, islands coalescence, Ostwald and inverse Ostwald ripening with a general simple kinetic Monte Carlo code," Thin Solid Films, 2010, 518, 5355-5361.

[DOI: 10.22068/ijmse.16.3.67]

41. Choy, T., "Effective medium theory: Principles and applications: Oxford University Press," 1999, 25-65.
42. Bruggeman, V. D., "Berechnung verschiedener physikalischer Konstanten von heterogenen Substanzen. I. Dielektrizitätskonstanten und Leitfähigkeiten der Mischkörper aus isotropen Substanzen," Annalen der physik, 1935, 416, 636-664.
43. Bruynooghe, S., Tonova, D., Sundermann, M., Koch, T., and Schulz, U., "Antireflection coatings combining interference multilayers and a nanoporous MgF2 top layer prepared by glancing angle deposition," Surface and Coatings Technology, 2015, 267, 40-44.
44. Anzengruber, S. W., Klann, E., Ramlau, R., and Tonova, D. "Numerical methods for the design of gradient-index optical coatings," Applied optics, 2012, 51, 8277-8295.
45. Hawkeye M. M. and Brett, M. J. "Glancing angle deposition: fabrication, properties, and applications of micro-and nanostructured thin films," Journal of Vacuum Science & Technology A, 2007, 25, 1317-1335.
46. Robbie, K., Brett, M. J., and Lakhtakia, A., "Chiral sculptured thin-films," Nature, 1996, 384, 616-616.
47. Tait, R., Smy, T., and Brett, M., "Modelling and characterization of columnar growth in evaporated films," Thin Solid Films, 1993, 226, 196-201.
48. Dervaux, J., Cormier, P., Konstantinidis, S., Moskovkin, P., Lucas, S., and Snyders, R., "Nanostructured Ti thin films by combining GLAD and magnetron sputtering: a joint experimental and modeling study." Thin Solid Films 636 ,2017, 644–657.
49. Godinho, V., Moskovkin, P., Álvarez, R., Caballero-Hernández, J., Schierholz, R., Bera, B., "On the formation of the porous structure in nanostructured a-Si coatings deposited by dc magnetron sputtering at oblique angles," Nanotechnology, 2014, 25, 355705.

[DOI: 10.22068/ijmse.16.3.67]